

Cohesive finite element modeling of age-related toughness loss in human cortical bone

Ani Ural, Deepak Vashishth*

*Department of Biomedical Engineering, Center for Biotechnology and Interdisciplinary Studies, Rensselaer Polytechnic Institute,
110 8th Street, Troy, NY 12180, USA*

Accepted 20 October 2005

Abstract

Although the age-related loss of bone quality has been implicated in bone fragility, a mechanistic understanding of the relationship is necessary for developing diagnostic and treatment modalities in the elderly population at risk of fracture. In this study, a finite element based cohesive zone model is developed and applied to human cortical bone in order to capture the experimentally shown rising crack growth behavior and age-related loss of bone toughness. The cohesive model developed here is based on a traction–crack opening displacement relationship representing the fracture processes in the vicinity of a propagating crack. The traction–displacement curve, defining the cohesive model, is composed of ascending and descending branches that incorporate material softening and nonlinearity. The results obtained indicate that, in contrast to initiation toughness, the finite element simulations of crack growth in compact tension (CT) specimens successfully capture the rising *R*-curve (propagation toughness) behavior and the age-related loss of bone toughness. In close correspondence with the experimentally observed decrease of 14–15% per decade, the finite element simulation results show a decrease of 13% in the *R*-curve slope per decade. The success of the simulations is a result of the ability of cohesive models to capture and predict the parameters related to bone fracture by representing the physical processes occurring in the vicinity of a propagating crack. These results illustrate that fracture mechanisms in the process zone control bone toughness and any modification to these would cause age-related toughness loss.

© 2005 Elsevier Ltd. All rights reserved.

Keywords: Cortical bone; Fracture toughness; Aging; Finite element method; Microcracking

1. Introduction

Age-related loss of bone quality has been implicated as a significant contributor to bone fragility (Burr et al., 1997) but it is still unknown how changes in bone quality alter the propensity of bone to fracture. Such a mechanistic understanding is essential for developing and evaluating approaches for diagnostic and treatment

modalities in the elderly population at risk of bone fracture.

Fracture mechanics approach has been commonly used to define the resistance of bone to fracture (for review see Bonfield, 1987; Melvin, 1993). These studies focused on a single parameter characterization of the fracture toughness including critical stress intensity factor and critical energy release rate. Melvin and Evans (1973) were among the first researchers to apply fracture mechanics to bovine bone by using a single-edge-notched (SEN) specimen. Following their study, Bonfield and Datta (1974) reported stress intensity factors using center-notched cylindrical (CNC) thin-walled tube specimens and SEN specimens for bovine bone (Bonfield and Datta, 1976). Wright and Hayes (1977)

*Corresponding author. Center for Biotechnology and Interdisciplinary Studies, Room 3137, Rensselaer Polytechnic Institute, 110 8th Street, Troy, NY 12180, USA. Tel.: +1 518 276 4050; fax: +1 518 276 3035.

E-mail addresses: urala@rpi.edu (A. Ural), vashid@rpi.edu (D. Vashishth).

demonstrated the first study using compact tension (CT) specimen configuration measuring fracture toughness of bovine femur. CT specimens were employed in subsequent studies on human and other cortical bone (Bonfield et al., 1978, 1984; Norman et al., 1992, 1995; Vashishth, 2004; Vashishth et al., 1997, 2000, 2004; Yeni and Norman, 2000; Yeni et al., 1997, 1998; Wang et al., 1998; Brown et al. 2000; Nalla et al., 2004b).

Another area of research interest involved determining the change in fracture toughness properties with age. Studies on age-related changes in these parameters showed a decreasing trend with age (Zioupos and Currey, 1998; Brown et al., 2000). Brown et al. (2000) measured the change in tensile and shear energy release rate values with age in human femur and tibia using CT specimens and compact shear specimens, respectively. They reported a significant decrease in tensile fracture toughness for both femur and tibia. Zioupos and Currey (1998) measured fracture toughness and J -integral energy needed to form a crack using human femur and also reported a significant decrease in both of these values.

In recent studies, propagation toughness, defined as the change in fracture toughness of bone as the crack progresses, is given more emphasis for characterizing fracture in bone. These studies showed that toughening mechanisms play an important role in the fracture behavior of bone by increasing its fracture resistance to crack propagation (Vashishth, 2004; Vashishth et al., 1997, 2000, 2003, 2004; Nalla et al., 2003, 2004a, b, 2005; Kahler et al., 2003; Malik et al., 2003). Toughening behavior in human cortical bone was experimentally shown in previous studies resulting in a rising crack growth (R -curve) behavior (Vashishth et al., 1997; Nalla et al., 2004b). In addition to the observed toughening behavior, experimental results also showed age-related loss of cortical bone toughness both in the initiation as well as in propagation toughness (Vashishth et al., 2004; Nalla et al., 2004b). The study by Vashishth et al. (1997) used CT specimen geometry to show the rising R -curve behavior in human tibia due to toughening mechanisms during crack growth. The same test procedure was used by Vashishth et al. (2004) to study the age-related changes in fracture toughness of cortical bone for subjects ranging from 34 to 97 years of age. In that study, the decrease in propagation toughness was found to be more pronounced than the decrease in initiation toughness. The same observation was reported by Nalla et al. (2004b) using CT specimens for human humerus where both initiation and propagation toughness decreased with age for the age range of 34–99 years.

The toughening behavior of bone reported in crack propagation tests is a result of the physical processes taking place in the vicinity of a propagating crack. The goal of this study is to present a computational model that represents the effects of these physical processes

and consequently captures the toughening behavior of bone and its age-related changes. Here, for the first time, we describe the development of a nonlinear finite element based cohesive model of bone fracture and demonstrate its successful application in capturing the experimentally measured rising R -curve behavior of human cortical bone (Vashishth et al., 1997; Nalla et al., 2004b) and age-related loss of bone toughness (Vashishth et al., 2004; Nalla et al., 2004b). Cohesive models have been a method of choice in engineering applications starting with the works of Dugdale (1960) and Barenblatt (1962) since they represent the physical processes occurring in the vicinity of a propagating crack by a simplified traction–displacement relationship and consequently isolate the fracture process from the surrounding continuum constitutive model. These applications varied from yielding in plastic plates (Dugdale, 1960) to cracking in concrete (Hillerborg et al., 1976), void nucleation in metallic materials (Needleman, 1987), plasticity effects in ductile materials, (Tvergaard and Hutchinson, 1992), dynamic fracture in brittle solids (Camacho and Ortiz, 1996; Ortiz and Pandolfi, 1999) and fatigue crack growth in metals (de Andres et al., 1999).

Our aim in this study is to develop a cohesive finite element model and show its predictive capability via crack growth simulations of CT specimens employing this model. Specifically, our goal is to demonstrate the rising R -curve behavior and age-related initiation and propagation fracture toughness loss in human cortical bone using a computational model based on independently measured parameters.

2. Methods

Crack growth simulations of CT specimens (Fig. 1a) were performed to capture the experimentally measured R -curve behavior and age-related loss of bone toughness in human cortical bone using the finite element method incorporating a cohesive model. The crack propagation is in the longitudinal direction (parallel to the long bone axis) as shown in Fig. 1(a). The cohesive model used here is similar to other models proposed in the engineering literature with an ascending and a descending branch making use of the effective traction and displacement concept which is a coupled representation of the normal and shear crack-opening displacements (Camacho and Ortiz, 1996, Ortiz and Pandolfi, 1999).

In the finite element approach, cohesive models can be implemented as interface elements that are compatible with regular solid finite elements. In two dimensions, the cohesive interface elements are composed of two line elements with zero thickness, which coincide in the reference configuration (Fig. 1b). Each line element has n nodes, which gives $2n$ nodes for the cohesive element.

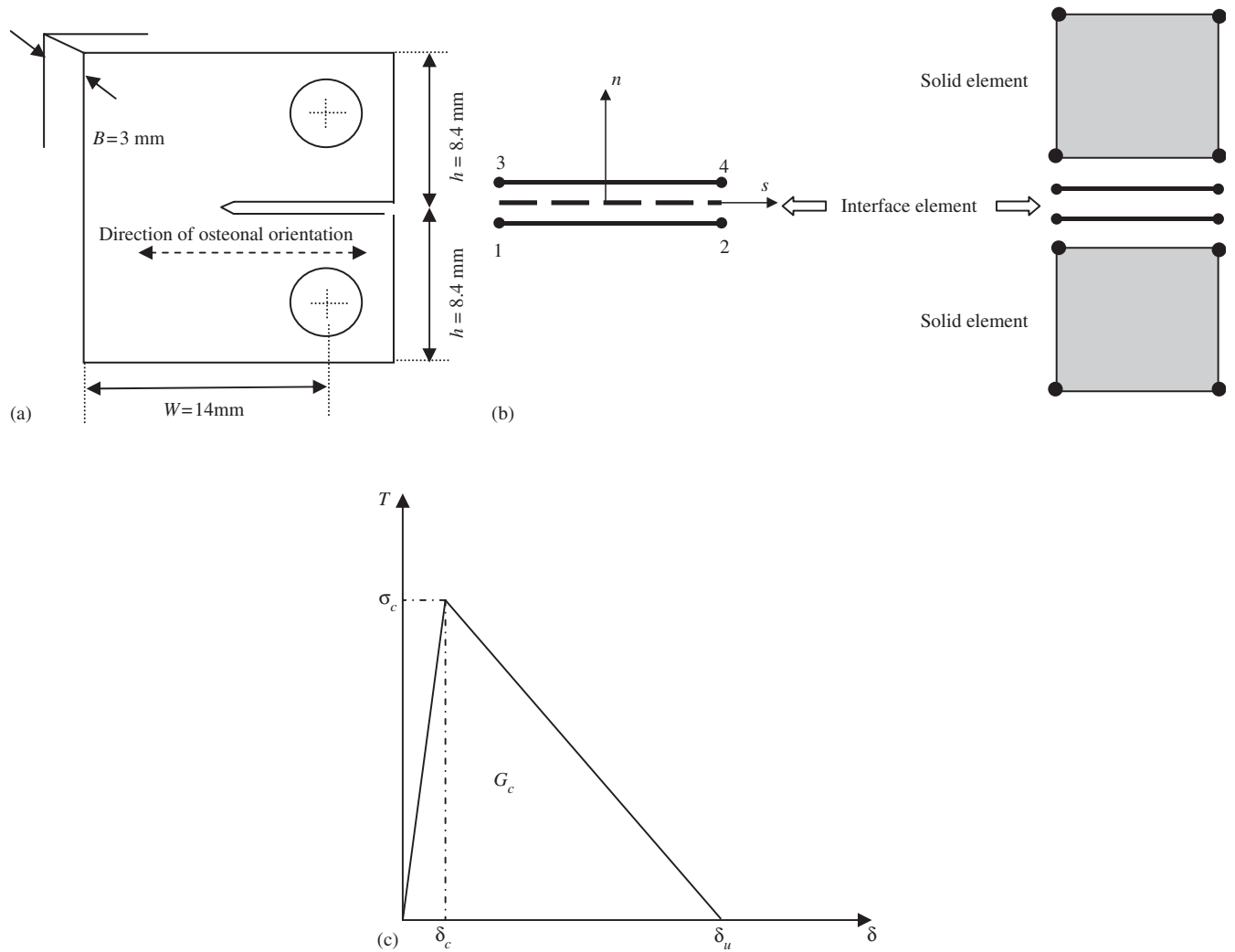


Fig. 1. (a) CT specimen for fracture toughness testing of human cortical bone. Note that $a/W = 0.52$ at the initial crack configuration. (b) Schematics of 2D, 4-noded cohesive element and its compatibility with solid elements. Note that the n and s axes denote the normal and tangential displacements of the cohesive element, respectively. (c) Traction–displacement relationship defining the cohesive zone model.

The finite element formulation of the cohesive model used in this study follows the work of Ortiz and Pandolfi (1999). According to this formulation, the traction is derived from a surface energy potential. This energy potential is dependent on the normal and shear opening of the surface and internal variables,

$$\phi = \phi(\delta_n, \delta_s, \mathbf{q}), \quad (1)$$

where, ϕ is the energy potential, δ_n is the relative displacement in the normal direction, $\delta_n = \boldsymbol{\delta} \cdot \mathbf{n}$, δ_s is the relative displacement in the shear direction, $\delta_s = |\boldsymbol{\delta}_s|$ and $\boldsymbol{\delta}_s = \boldsymbol{\delta} - \delta_n \mathbf{n}$, \mathbf{q} is a collection of internal state variables, \mathbf{n} is the unit normal of the interface element, and $\boldsymbol{\delta}$ is the displacement vector. The cohesive traction, \mathbf{t} , is then calculated as

$$\mathbf{t} = \frac{\partial \phi}{\partial \boldsymbol{\delta}}, \quad (2)$$

$$\mathbf{t} = \frac{\partial \phi}{\partial \delta_n}(\delta_n, \delta_s, \mathbf{q}) \mathbf{n} + \frac{\partial \phi}{\partial \delta_s}(\delta_n, \delta_s, \mathbf{q}) \frac{\boldsymbol{\delta}_s}{\delta_s}. \quad (3)$$

The formulation of the cohesive traction is simplified even further with introduction of a coupled opening displacement. The effective opening displacement is defined as

$$\delta = \sqrt{\eta^2 \delta_s^2 + \delta_n^2}, \quad (4)$$

where η is a nondimensional factor that couples the normal and shear effects ($0 \leq \eta \leq 1$). The traction expression can be rewritten as

$$\mathbf{t} = \frac{T}{\delta} (\eta^2 \boldsymbol{\delta}_s + \delta_n \mathbf{n}), \quad (5)$$

$$T = \frac{\partial \phi}{\partial \delta}(\delta, \mathbf{q}), \quad (6)$$

$$T = \sqrt{\eta^{-2} |t_s|^2 + t_n^2}, \quad (7)$$

where T is the scalar effective traction, δ is the scalar effective opening displacement, t_n is the normal component of the traction vector, $|t_s|$ is the resultant of the shear tractions.

The relationship between the effective traction and effective opening displacement is defined by three parameters, two of which uniquely define the fracture process. These parameters are the peak traction (local strength of the material, σ_c), a characteristic opening displacement at fracture (δ_u), and the energy needed for opening the crack (area under the traction–displacement curve, G_c) (Fig. 1c). The crack can be considered traction free when the opening displacement reaches the characteristic opening, δ_u . There are various types of traction–displacement relationships proposed in the literature to model the fracture process including linear and exponential relationships (Needleman, 1987; Ortiz and Pandolfi, 1999; de Andres et al., 1999). The shape of the cohesive relationship, however, has little effect on the resulting fracture behavior (Tvergaard and Hutchinson, 1992). Therefore, in this study, we employed a simple bilinear traction–displacement curve of the following form:

$$T = \begin{cases} \frac{\sigma_c}{\delta_c} \delta, & \delta \leq \delta_c, \\ \sigma_c \frac{(\delta_u - \delta)}{(\delta_u - \delta_c)}, & \delta_c < \delta \leq \delta_u, \\ 0, & \delta \geq \delta_u, \end{cases} \quad (8)$$

where T and δ are the scalar-effective traction and opening displacement as defined above, σ_c is the peak traction representing the maximum strength of the cohesive model, δ_c is the critical displacement at which the crack initiates and δ_u is the failure displacement when a complete crack forms. This model allows for the extension of crack as a result of the traction–displacement curve. Each cohesive element follows the traction–crack opening profile described above and cracks when there is no transfer of traction between the opening surfaces (i.e. $T = 0$ and $\delta = \delta_u$). The extent of the process zone is determined by the number of elements that are activated and undergo softening. It is important to note that the initial slope in the model is mainly required to avoid numerical problems between the cohesive elements and the surrounding continuum (Cornec et al., 2003). Thus, the critical displacement (δ_c), at which the crack initiates is not a physical quantity and should be chosen as small as possible. For this study, it was chosen to be 0.00175 mm and was kept constant for all simulations.

A finite element model of the CT specimens (Vashishth et al., 1997, 2004) was created using a finite element program, FEAP (v7.1, 1999), composed of quadrilateral elements (Fig. 2). The cohesive interface elements are placed in the direction of the expected crack growth as shown in Fig. 2. In the current model, input parameters are σ_c , the ultimate strength in the transverse direction (perpendicular to the osteonal direction along which the crack growth occurs), and

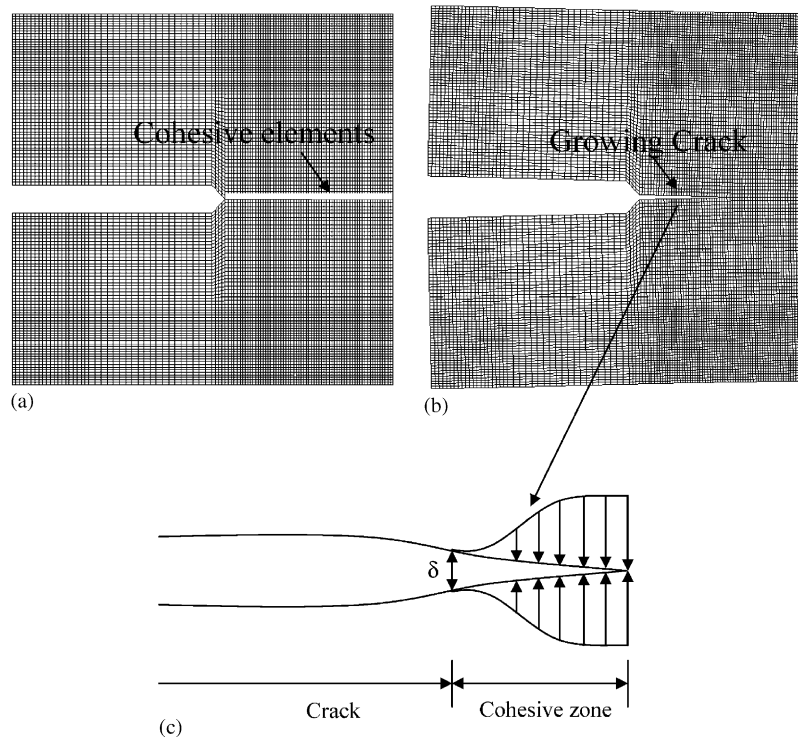


Fig. 2. (a) An undeformed finite element mesh of CT specimen showing the location of the cohesive elements marked by the white line (b) a deformed mesh of CT specimen with a propagating crack. Note that displacement magnification factor is 5. (c) A schematic representation of the cohesive zone.

G_c , the energy release rate of cortical bone. As described above, these two parameters are sufficient to define a unique traction–separation relationship. The values of G_c and σ_c used in the simulations are obtained from the experimental results reported in literature (Brown et al., 2000; Reilly and Burstein, 1975). Specifically, the change in G_c of human tibia with age was determined from the CT test data reported in Brown et al. (2000) for the age range of 50–90 years (Table 1). There is very limited data available in the literature on the age-related change of ultimate strength of human cortical bone in transverse direction. An estimate of the change in the transverse ultimate strength properties of human tibia was obtained by a linear fit through the values reported in Reilly and Burstein (1975) for human femur (Table 1). δ_u is the third parameter in the model dependent on σ_c and G_c and can be calculated using the definition of the traction–displacement curve. The corresponding δ_u values are also listed in Table 1.

The continuum material is modeled as a linear elastic orthotropic material. The set of material properties used in the simulations are taken from Knets (1978) and are listed in Table 2. These values were kept constant in the simulations for all ages since the age-related changes in the elastic properties reported in the literature (Burstein et al., 1976; McCalden et al., 1993) is not significant compared to the changes in the fracture mechanics properties. The simulations were carried out under plane strain assumptions. The load and crack growth data computed in the simulations were used to calculate the crack growth resistance (K_R) at various crack lengths using the equation given in ASTM E399-90 (2000):

$$K_R = \frac{P}{BW^{1/2}} f\left(\frac{a}{W}\right), \quad (9)$$

$$f(a/W) = \frac{(2 + (a/W))(0.886 + 4.64(a/W) - 13.32(a/W)^2 + 14.72(a/W)^3 - 5.6(a/W)^4)}{(1 - (a/W))^{3/2}}, \quad (10)$$

where P is the load, a is the crack length, W is the width of the specimen from the load line, and B is the thickness. For each donor group, K_R is plotted as a function of square root of crack growth, (defined as R -curve) to obtain the resulting slope (defined as R -curve slope) by linear regression. The R -curve slope was calculated for crack extensions from 0.25 to 2.25 mm in the simulations following the experimental procedure (Vashishth et al., 1997, 2004).

3. Results

3.1. Mesh size

Cohesive elements are traditionally known for their mesh dependent characteristics. A mesh sensitivity study

Table 1

Cohesive model parameters (energy release rate, transverse ultimate strength and characteristic effective crack opening displacement) used in the simulations. The energy release rate (G_c) and transverse ultimate strength values (σ_c) are calculated based on the experimental data from Brown et al. (2000) and Reilly and Burstein (1975), respectively. The relationship defining the variation of mode I fracture toughness in human tibia with age (age range 50–90 years) was found as $G_c = -13.42 \text{ Age} + 1379.19$ by Brown et al. (2000). Note that the unit associated to G_c in this equation is N/m. The transverse ultimate strength values for different ages reported in Reilly and Burstein (1975) for human femur were plotted and a linear fit was made through these points giving the equation $\sigma_c = -0.4338 \text{ Age} + 65.184$. The values of characteristic effective crack opening displacement were calculated from G_c and σ_c that are given in the first and second columns. The constant value of δ_c used in all simulations is 0.00175 mm. δ_c is small compared to all δ_u

Age	G_c (N/mm)	σ_c (MPa)	δ_u (mm)
50	0.71	43.5	0.033
60	0.57	39.2	0.029
70	0.44	34.8	0.025
80	0.31	30.5	0.020
90	0.17	26.1	0.013

was carried out by increasing the number of cohesive elements resolving the process zone. Fig. 3 shows the change in the R -curve slope with respect to the mesh size as well as the curve fit that indicates convergence of the values. As seen in Fig. 3, the last mesh sizes showed convergence, therefore, the cohesive element size was chosen as 37.5 μm .

3.2. Material assumptions

As mentioned above, the simulations were performed using orthotropic material properties shown in Table 2.

In order to investigate the difference that would be introduced in the simulations with the use of an isotropic material assumption, FEM simulations were carried out for the age group of 50 years using isotropic and orthotropic bone properties. The effective isotropic properties were calculated using the orthotropic bone properties listed in Table 2 following the method defined in Cowin (1989) and Cowin and Sadeh (1991). The method described in these studies included the calculation of upper and lower bounds of bulk modulus and shear modulus from the stiffness matrix of an orthotropic material. The effective isotropic elastic modulus was characterized by the average values of these upper and lower bounds. The change in the fracture toughness behavior of the bone using the effective isotropic material properties listed in Table 2 is shown in Fig. 4.

Table 2

Orthotropic and effective isotropic material properties used in the simulations for all age groups

Orthotropic properties of human tibia (Knets, 1978)

E_1	18.4 GPa
E_2	8.5 GPa
E_3	6.9 GPa
G_{12}	4.9 GPa
G_{23}	2.4 GPa
G_{31}	3.6 GPa
ν_{13}	0.32
ν_{23}	0.62
ν_{12}	0.31

Effective isotropic properties of human tibia

E	10.0 GPa
ν	0.33

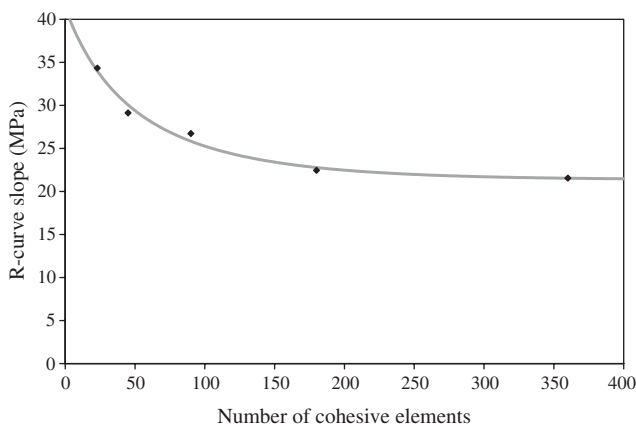


Fig. 3. Change in R -curve slope with respect to the number of cohesive elements used in the FEM model. The solid diamond labels show the simulation results and solid gray line is the nonlinear curve fit defined by the equation $y = a(b - a)/(be^{cx(b-a)} - a)$ where $a = 41.31340$, $b = 19.94795$ and $c = 0.00053$. Regression coefficient (r^2) for the curve fit is 0.98.

The simulation results showed that isotropic material assumption resulted in lower crack initiation (13% decrease) and propagation (45% decrease) toughness.

3.3. Toughness predictions

Finite element simulations of CT specimens were carried out using the parameters corresponding to ages 50–90 years. The finite element simulations of CT tests showed a rising R -curve behavior. Fig. 5(a) shows the plot of R -curves for 50, 70 and 90 years obtained from FEM simulations. As expected, the toughness increased as the crack propagated. On the other hand the values of load required for crack propagation decreased with increasing age (Fig. 5b). This figure indicates that with age an equivalent amount of crack growth was attained

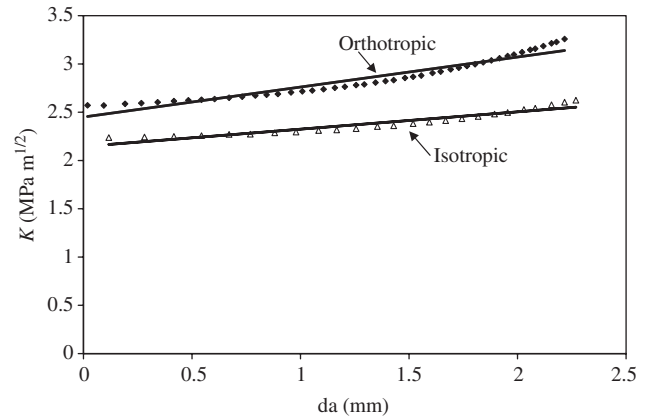


Fig. 4. FEM simulation of R -curve behavior under orthotropic and effective isotropic material assumptions for the age of 50 years. Linear regression coefficients (r^2) for the orthotropic and isotropic FEM simulation results are 0.93 and 0.91, respectively. The orthotropic material properties are taken from Knets (1978) and effective isotropic properties were calculated using the orthotropic bone properties following the method defined in Cowin (1989) and Cowin and Sadeh (1991).

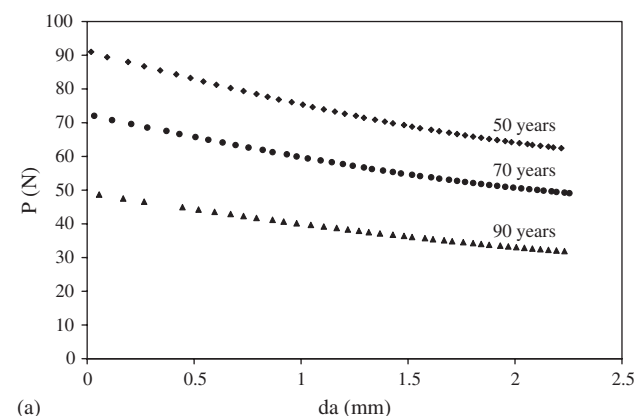
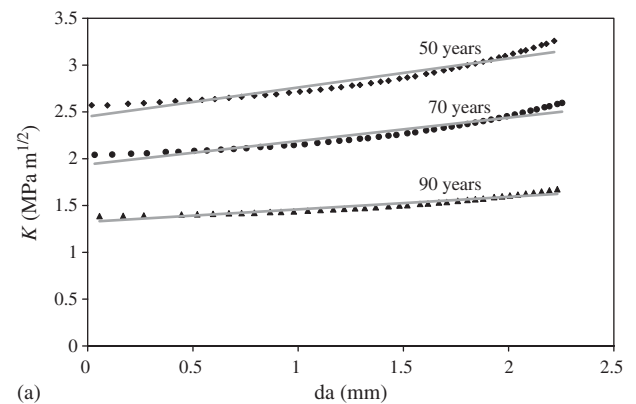


Fig. 5. (a) FEM simulations demonstrate a linear increase in crack growth resistance (K_R) vs. crack extension. The coefficients of linear regression (r^2) for 50, 70 and 90 years donors, shown above, are 0.93, 0.93 and 0.92, respectively. (b) FEM simulations demonstrate that a lower level of load is required to attain the same crack length as the age increases.

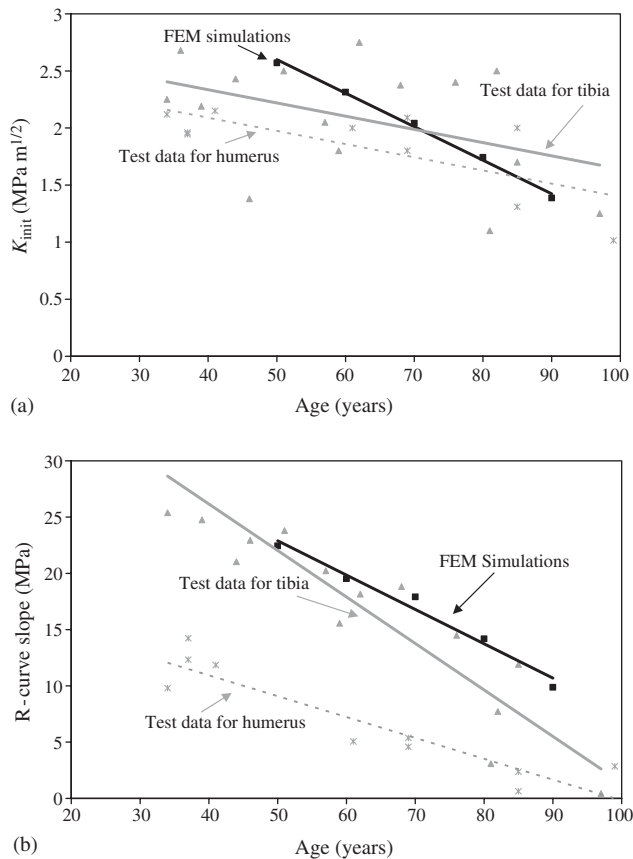


Fig. 6. (a) FEM simulation of age-related initiation toughness loss and its comparison with experimental results. Note that the black squares denote the simulation results whereas gray triangles and stars denote experimental results for tibia (Vashishth et al., 2004) and humerus (Nalla et al., 2004a, b), respectively. The straight lines show the linear regression of the data and are given by the equations $K_{init,tibia} = 2.7985 - 0.0116 \text{ Age}$, $K_{init,humerus} = 2.551 - 0.0115 \text{ Age}$ and $K_{init,FEM} = 4.0687 - 0.0294 \text{ Age}$. Linear regression coefficients (r^2) for of the test data for tibia, humerus and FEM simulations are 0.19, 0.52 and 0.99, respectively. (b) FEM simulation of age-related propagation toughness loss and its comparison with experimental results. Note that the black squares denote the simulation results whereas gray triangles and stars denote experimental results for tibia (Vashishth et al., 2004) and humerus (Nalla et al., 2004a, b), respectively. The straight lines show the linear regression of the data and are given by the equations $R_{tibia} = 42.692 - 0.4131 \text{ Age}$, $R_{humerus} = 18.358 - 0.1856 \text{ Age}$ and $R_{FEM} = 38.146 - 0.305 \text{ Age}$. Linear regression coefficients (r^2) of the test data for tibia, humerus and FEM simulations are 0.85, 0.85 and 0.98, respectively.

with a lower level of load as a result of the less amount of energy needed for propagating a crack.

The initiation toughness of CT tests showed a decreasing trend with increasing age. Fig. 6(a) shows the decreasing trend observed in the simulations and its comparison with the experimental data reported in the literature. The initiation toughness decreased 11% per decade in the simulations compared to the 5% decrease in both tibia (Vashishth et al., 2004) and humerus (Nalla et al., 2004b) test results.

Fig. 6(b) shows the FEM computed age-related propagation toughness loss and its comparison with the experimental results reported in the literature. The FEM-based cohesive model successfully captured the decreasing trend in the R -curve slope with age. The FEM simulations predicted a decrease of 13% in the R -curve slope per decade close to the 14% decrease reported in the experiments carried out using tibia (Vashishth et al., 2004) and 15% decrease per decade for humerus (Nalla et al., 2004b) (Fig. 6b).

4. Discussion

This study demonstrates the feasibility of using finite element based cohesive models to capture and predict the processes and parameters related to bone fracture. The predictions are based on independently measured parameters in the literature, which are used to define the parameters of the cohesive model. Consistent with experimental results (Vashishth et al., 1997, 2004; Nalla et al., 2004b), finite element simulations of crack propagation tests demonstrated a rising R -curve with crack extension (Fig. 5a) and predicted a greater age-related loss in propagation than initiation toughness (Fig. 6). These successful simulation results show the ability of cohesive models to take into account the physical processes occurring in the vicinity of the crack tip. In this study, the cohesive energy is assumed to be equal to the energy released at the onset of stable crack extension, and the critical load at which the softening starts is assumed to be the ultimate strength of the material. These globally measured values are considered to be valid representations of the fracture behavior of bone in the process zone because the cohesive model is a phenomenological characterization of the overall behavior of the material and does not try to match the point wise behavior.

In this study, linear elastic fracture mechanics (LEFM) approach is replaced by a cohesive model, which is capable of simulating nonlinear behavior at the process zone. In cohesive models, both crack initiation and crack growth are dependent on the parameters defining the traction–separation relationship as well as the continuum properties. Moreover, these parameters are phenomenological characterizations of the process zone surrounding the crack tip and can be easily deduced from simple experiments. The strength of the model comes from its capability to predict and investigate change in propagation toughness using information derived from simple experiments related to strength and bulk toughness of bone.

However, it is important to note that the finite element simulation results are dependent on the model parameters. As pointed out previously, there is very limited experimental data on the age-related change in

the transverse ultimate properties of human tibia. Therefore, the values used in the simulations are an estimate of how this value changes with age. The discrepancies between experimental and simulation results can result from this limited data in the literature. A more thorough experimental evaluation of the change of transverse ultimate strength with age will improve the prediction capabilities of the model both for initiation and propagation toughness. It is also important to note that the microstructural features of the cortical bone, such as cement lines, lamellae and pores, were not explicitly modeled in the simulations.

The simulations showed a significant change introduced by using effective isotropic material properties instead of orthotropic properties for bone. As shown in Fig. 4, there is a significant decrease in the initiation toughness as well as in the *R*-curve slope predicted by the isotropic model. This indicates that using an isotropic model results in an overly conservative estimation of the load needed to initiate and propagate a crack.

The initiation toughness shows a steeper change in the simulations compared to the experiments (Vashishth et al., 2004; Nalla et al., 2004b). The finite element CT model represents the location of the initial crack but it cannot capture the changes introduced in the vicinity of the initial notch due to machining. The effects of initial notch machining combined with the choice of model parameters described above can be the cause of the difference in the experimentally observed and computationally predicted decrease in initiation toughness. Although, not as pronounced as the experimental data, the age-related loss of initiation toughness predicted by the simulations is lower than the decrease in propagation toughness.

Finite element simulations successfully predicted the age-related decrease in fracture toughness as shown in Fig. 6(b). The percent change in the *R*-curve slope per decade as well as the values of the *R*-curve slopes are similar both in the experiments and simulations. The experimental data given in Nalla et al. (2004b) showed much lower *R*-curve values compared both to the experiments (Vashishth et al., 2004) and simulations. As pointed out by the authors (Nalla et al., 2004b), their studies were based on cortical bone from a different anatomical location which can result in significant discrepancies. The parameters for the simulations were determined from the data present in the literature for tibia, therefore, it is consistent to compare the simulation results to tibia test data reported by Vashishth et al. (2004).

The toughening behavior shown by the simulations in this study and by experimental data in Vashishth et al. (2004) and Nalla et al. (2004b) is a result of processes including microcracking and/or crack bridging. The computational model developed here provides a predic-

tion tool for fracture behavior of cortical bone by representing the process zone and its effect on the propagating crack. Specifically, this model allows for capturing the change in the fracture properties of bone with aging. The age-related changes in the overall toughness properties of the bone can be predicted through the localized changes in the fracture behavior occurring in the vicinity of a crack. These changes are reflected in the input parameters of the cohesive model and are incorporated in the simulations to allow for the prediction of bone fracture toughness. Combining computational methods with experimental results can provide a further mechanistic understanding of fracture processes in cortical bone including the interaction and relative contributions of different toughening mechanisms and their relationship with age. The computational approach presented here can be extended to investigate the underlying mechanisms that result in toughening behavior and the contribution of different toughening mechanisms to crack growth in cortical bone.

It is noteworthy that, based on a small subset of the material parameters related to the process zone, the FEM-based cohesive model developed in this study was successful in predicting the age-related loss of bone toughness (Fig. 6b). Events and fracture mechanisms in the process zone including microcracking and/or crack bridging therefore provide a mechanistic basis of bone toughness and any modification of these would cause age-related toughness loss and increase fracture risk in the elderly.

Acknowledgments

This work is supported by National Institutes of Health Grant AR49635.

References

- ASTM E399-90, 2000. Standard Test Method for Plane-strain Fracture Toughness of Metallic Materials. American Society for Testing and Materials, Philadelphia.
- Barenblatt, G.I., 1962. The mathematical theory of equilibrium of cracks in brittle fracture. *Advances in Applied Mechanics* 7, 55–129.
- Bonfield, W., 1987. Advances in the fracture mechanics of cortical bone. *Journal of Biomechanics* 20, 1071–1081.
- Bonfield, W., Datta, P.K., 1974. Impact fracture of compact bone in a shock tube. *Journal of Material Science* 9, 1609–1614.
- Bonfield, W., Datta, P.K., 1976. Fracture toughness of compact bone. *Journal of Biomechanics* 9, 131–134.
- Bonfield, W., Grynblas, M.D., Young, R.J., 1978. Crack velocity and the fracture of bone. *Journal of Biomechanics* 11, 473–479.
- Bonfield, W., Behiri, J.C., Charalambides, B., 1984. Orientation and age-related dependence of the fracture toughness of cortical bone. In: Perren, S.M., Schneider, E. (Eds.), *Biomechanics: Current Interdisciplinary Research*. Martinus Nijhoff, Dordrecht, pp. 185–189.

- Brown, C.U., Yener, Y., Norman, T.L., 2000. Fracture toughness is dependent on bone location—a study of femoral neck, femoral shaft, and the tibial shaft. *Journal of Biomedical Materials Research* 49, 380–389.
- Burr, D.B., Forwood, M.R., Fyhrie, D.P., Martin, R.B., Schaffler, M.B., Turner, C.H., 1997. Bone microdamage and skeletal fragility in osteoporotic and stress fractures. *Journal of Bone and Mineral Research* 12, 6–15.
- Burstein, A.H., Reilly, D.T., Martens, M., 1976. Aging of bone tissue: mechanical properties. *The Journal of Bone and Joint Surgery* 58A, 82–86.
- Camacho, G.T., Ortiz, M., 1996. Computational modeling of impact damage in brittle materials. *International Journal of Solids and Structures* 33, 2899–2938.
- Cornec, A., Scheider, I., Schwalbe, K.-H., 2003. On the practical application of the cohesive model. *Engineering Fracture Mechanics* 70, 1963–1987.
- Cowin, S.C., 1989. Properties of the anisotropic elasticity tensor. *Quarterly Journal of Mechanics and Applied Mathematics* 42, 249–266.
- Cowin, S.C., Sadegh, A.M., 1991. Non-interacting modes for stress, strain and energy in anisotropic hard tissue. *Journal of Biomechanics* 24, 859–867.
- de Andres, A., Perez, J.L., Ortiz, M., 1999. Elastoplastic finite element analysis of three-dimensional fatigue crack growth in aluminum shafts subjected to axial loading. *International Journal of Solids and Structures* 36, 2231–2258.
- Dugdale, D.S., 1960. Yielding of steel sheets containing slits. *Journal of the Mechanics and Physics of Solids* 8, 100–104.
- FEAP Version 7.1. A Finite Element Analysis Program, Robert L. Taylor, 1999.
- Hillerborg, A., Modeer, M., Petersson, P.E., 1976. Analysis of crack formation and crack growth in concrete by means of fracture mechanics and finite elements. *Cement and Concrete Research* 6, 773–782.
- Kahler, B., Swain, M.V., Moule, A., 2003. Fracture-toughening mechanism responsible for differences in work to fracture of hydrated and dehydrated dentine. *Journal of Biomechanics* 36, 229–237.
- Knets, I.V., 1978. Mechanics of biological tissues. A review. *Polymer Mechanics* 13, 434–440.
- Malik, C.L., Stover, S.M., Martin, R.B., Gibeling, J.C., 2003. Equine cortical bone exhibits rising *R*-curve fracture mechanics. *Journal of Biomechanics* 36, 191–198.
- McCalden, R.W., McGeough, J.A., Barker, M.B., Court-Brown, C.M., 1993. Age-related changes in the tensile properties of cortical bone. *The Journal of Bone and Joint Surgery* 75A, 1193–1205.
- Melvin, J.W., 1993. Fracture mechanics of bone. *Journal of Biomechanical Engineering* 115, 549–554.
- Melvin, J.W., Evans, F.G., 1973. Crack propagation in bone. 1973 Biomechanics Symposium. ASME, New York, pp. 87–88.
- Nalla, R.K., Kinney, J.H., Ritchie, R.O., 2003. Mechanistic fracture criteria for the failure of human cortical bone. *Nature Materials* 2, 164–168.
- Nalla, R.K., Kruzic, J.J., Ritchie, R.O., 2004a. On the origin of the toughness of mineralized tissue: microcracking or crack bridging? *Bone* 34, 790–798.
- Nalla, R.K., Kruzic, J.J., Kinney, J.H., Ritchie, R.O., 2004b. Effect of aging on the toughness of human cortical bone: evaluation by *R*-curves. *Bone* 35, 1240–1246.
- Nalla, R.K., Kruzic, J.J., Kinney, J.H., Ritchie, R.O., 2005. Mechanistic aspects of fracture and *R*-curve behavior in human cortical bone. *Biomaterials* 26, 217–231.
- Needleman, A., 1987. A continuum model for void nucleation by inclusion debonding. *Journal of Applied Mechanics* 54, 525–531.
- Norman, T.L., Vashishth, D., Burr, D.B., 1992. Effect of groove on bone fracture toughness. *Journal of Biomechanics* 25, 1489–1492.
- Norman, T.L., Vashishth, D., Burr, D.B., 1995. Fracture toughness of human bone under tension. *Journal of Biomechanics* 28, 309–320.
- Ortiz, M., Pandolfi, A., 1999. Finite-deformation irreversible cohesive elements for three-dimensional crack propagation analysis. *International Journal for Numerical Methods in Engineering* 44, 1267–1282.
- Reilly, D.T., Burstein, A.H., 1975. The elastic and ultimate properties of compact bone tissue. *Journal of Biomechanics* 8, 393–405.
- Tvergaard, V., Hutchinson, J.W., 1992. The relation between crack growth resistance and fracture process parameters in elastic-plastic solids. *Journal of the Mechanics and Physics of Solids* 40, 1377–1397.
- Vashishth, D., 2004. Rising crack-growth-resistance behavior in cortical bone: implications for toughness measurements. *Journal of Biomechanics* 37, 943–946.
- Vashishth, D., Behiri, J.C., Bonfield, W., 1997. Crack growth resistance in cortical bone: concept of microcrack toughening. *Journal of Biomechanics* 30, 763–769.
- Vashishth, D., Tanner, K.E., Bonfield, W., 2000. Contribution, development and morphology of microcracking in cortical bone during crack propagation. *Journal of Biomechanics* 33, 1169–1174.
- Vashishth, D., Tanner, K.E., Bonfield, W., 2003. Experimental validation of a microcracking-based toughening mechanism for cortical bone. *Journal of Biomechanics* 36, 121–124.
- Vashishth, D., Wu, P., Gibson, G. J., 2004. Age-related loss in bone: toughness is explained by non-enzymatic glycation of collagen. *Transactions of the 50th Annual Meeting of the Orthopaedic Research Society*. #497, San Francisco, CA.
- Wang, X.D., Masilamani, N.S., Mabrey, J.D., Alder, M.E., Agrawal, C.M., 1998. Changes in the fracture toughness of bone may not be reflected in its mineral density, porosity, and tensile properties. *Bone* 23, 67–72.
- Wright, T.M., Hayes, W.C., 1977. Fracture mechanics parameters for compact bone—effects of density and specimen thickness. *Journal of Biomechanics* 10, 419–430.
- Yeni, Y.N., Norman, T.L., 2000. Fracture toughness of human femoral neck: effect of microstructure, composition, and age. *Bone* 26, 499–504.
- Yeni, Y.N., Brown, C.U., Wang, Z., Norman, T.L., 1997. The influence of bone morphology on fracture toughness of the human femur and tibia. *Bone* 21, 453–459.
- Yeni, Y.N., Brown, C.U., Norman, T.L., 1998. The influence of bone composition and apparent density on fracture toughness of the human femur and tibia. *Bone* 22, 79–84.
- Zioupou, P., Currey, J.D., 1998. Changes in the stiffness, strength, and toughness of human cortical bone with age. *Bone* 22, 57–66.